THROUGH WALL RADAR IMAGING USING UWB NOISE WAVEFORMS

Ram M. Narayanan

Department of Electrical Engineering
The Pennsylvania State University
University Park, PA 16802

ABSTRACT

This paper examines the results of our research on the use of ultrawideband noise waveforms for imaging objects behind walls. The advantages of using thermally generated noise as a probing signal are introduced. The technique of heterodyne correlation, used to inject coherence in the random noise probing signal and to collapse the wideband reflected signal into a single frequency, is presented. We address issues related to locating, detection, and tracking humans behind walls using the Hilbert-Huang Transform approach for human activity characterization. The results indicate that noise radar technology combined with modern signal processing approaches is indeed a viable technique for covert high-resolution imaging of obscured stationary and moving targets.

***Index Terms*—** Heterodyne correlation, Hilbert-Huang Transform, noise radar, through wall imaging, ultrawideband

1. INTRODUCTION

Systems built on existing technology for through-wall sensing for anti-terrorism and earthquake rescue applications are heavy and inconvenient to deploy and operate in the field. The software defined radio (SDR) concept has provided a novel solution for advancing current technology to a new generation of systems that import appropriate digital techniques. The software defined radio was first proposed in 1989 [1] and it has been widely used in new wireless technology, such as third generation mobile phone, global positioning systems (GPS), and other personal communication tools. SDR techniques have also provided new ideas for the design of modern radar systems that are reliable, compact, and light-weight. Considerable improvement in system performance has been observed compared to conventional radar. The model-based approach minimizes the differences between simulation and the measurement by using the SDR concept. Such architectures can be realized by powerful analog-to-digital converters (ADCs) and state-of-the-art digital signal processing technology. Radio frequency (RF) front-end circuits can be replaced by digital integrated circuit components, thereby reducing the size and weight of the radar system. Implementation of short-pulse or wideband frequency-modulated radar systems is relatively expensive for through-wall surveillance (TWS) applications.

To confound detection, continuous-wave UWB random noise radar technology is an ideal solution. The technique works by transmitting a random noise waveform and cross-correlating the reflected echoes with a time-delayed replica of the transmit signal. Random noise signals are inherently difficult to detect and jam since they are featureless [2]. Since UWB radars used for TWS applications are typically in the UHF range (500-1000 MHz) for good penetration through building wall materials, chip-based arbitrary signal generators can be used as noise sources and field programmable gate arrays (FPGAs) can be used for time-delay and cross-correlation implementation, thereby achieving a total digital radar solution. The major challenge is to develop a simplified architecture which will reduce cost without sacrificing performance. Preliminary simulations indicate that we can use 2-bit signal quantization which would permit more rapid range scanning by the FPGA. In addition to locating and tracking both moving and stationary humans through various interior and exterior building walls, the capability to identify inanimate objects (such as furniture) is also desirable.

2. ADVANTAGES OF USING NOISE WAVEFORMS

Effective radar surveillance in a hostile setting requires covert and interference-free operation in a spectrally dense environment. Most low probability of intercept (LPI) and low probability of detection (LPD) waveforms primarily rely upon the use of pseudorandom transmit waveforms. With the increasing storage and computational capabilities of advanced digital signal processors, it is easy to detect, characterize, recognize, and jam such signals. Random noise radar, which transmits incoherent thermally-generated noise [3], [4], is an attractive and viable option in these applications. The reflected signal from the target is cross-correlated with a time-delayed replica of the transmit waveform. When the internal delay equals the round-trip time to the target, a peak is obtained in the correlation signal; otherwise, the correlator output is zero. The range resolution ΔR is inversely proportional to the transmit bandwidth B and is given by $\Delta R = c/2B$, where c is the speed of light. Thus, a 500-MHz bandwidth yields an acceptable 30-cm (1-foot) range resolution.

Major advantages and features of UWB noise radar are:

• *Frequency diversity*: Since the instantaneous noise waveform is spread over a wide frequency range, it has the necessary diversity to reduce clutter and multipath effects.

• *Immunity from detection*: Since the waveform is not repeatable and spread over a wide band, it does not appear as an intentional signal on the adversary's receiver.

• *Immunity from jamming and interference*: External signals caused by jammers or other interfering transmitters will not correlate with the time-delayed transmit replica and hence will yield zero at the correlator output.

• *Cost-effectiveness*: Since thermal noise is easy to generate, expensive modulators with good linearity or antennas with good impulse responses are not needed.

• *Spectral efficiency*: Many noise radars can occupy the same spectral band with negligible cross-interference as one radar's signal will not correlate with another radar's transmit replica.

• *Frequency shaping*: Filtering can be used to adaptively shape the transmit noise spectrum to reduce clutter and enhance detection of specific target types, prevent signal leakage into adjacent spectral bands, or prevent in-band spectral fratricide with friendly systems.

• *Thumbtack range-Doppler ambiguity function*: Noise radars can achieve high resolution in both range and Doppler which can be independently controlled by varying the bandwidth and integration time respectively.

• *Operational readiness*: Noise radar technology has entered the realm of operational readiness following extensive field-testing of several systems around the world.

• *Technology maturity*: Current noise radar technology is fully mature for short-range applications (less than 1 km). Thus, they are ideally suited for covert close-range applications such as through-wall imaging, mine detection, and detection of concealed weapons through clothing.

• *Noise source reliability*: Low-power solid state noise sources are extremely reliable and have been extensively used in broadband communications receiver testing.

3. THEORY OF NOISE RADAR

We propose a time-frequency model for the transmit noise waveform, represented as

$$v_t(t) = a(t)\cos\{[\omega_0 + \delta\omega]t\} \tag{1}$$

where $a(t)$ is the Rayleigh distributed amplitude and $\delta\omega(t)$ is the uniformly distributed frequency $[-\Delta\omega \le \delta\omega \le +\Delta\omega]$. Assuming $a(t)$ and $\delta\omega(t)$ are uncorrelated, the average power in the signal is $<a^2(t)>/2R_0$, where R_0 is the system impedance. The center frequency f_0 and the bandwidth B are $\omega_0/2\pi$ and $\Delta\omega/\pi$ respectively. A signal is considered narrowband if the fractional bandwidth B/f_0 is less than 10% and ultrawideband (UWB) if it is greater than 25%. Although the time-frequency representation, shown in equation (1) is inherently narrowband, we extend it to the UWB case owing to its simplicity and ease of signal analysis.

A block diagram of a basic noise radar system is shown in Figure 1. This is called a homodyne correlation noise radar since the correlation process downconverts the received signal to DC for a stationary target and to the Doppler frequency for a moving target. In this scheme, the reflected signal is correlated with a time-delayed replica of the transmit signal. If the roundtrip time delay to the target matches the internal time delay, a peak is observed in the correlator whose magnitude is proportional to the target reflectivity. The internal time delay then yields the range to the target. The mixer followed by a low pass filter acts as the correlator.

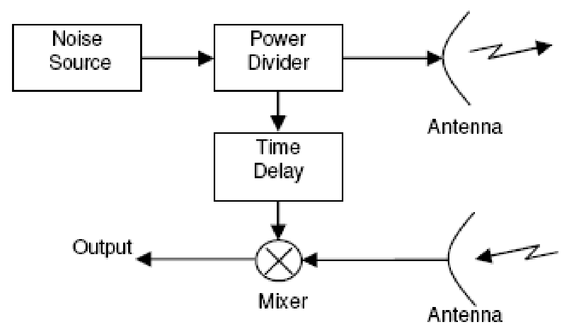

Figure 1: Block diagram of a homodyne correlation noise radar.

If the target complex reflectivity $\overline{\Gamma}$ is $\Gamma\exp(j\Theta)$, the reflected signal $v_r(t)$ is given by

$$v_r(t) = \Gamma a(t - t_0)\cos\{[\omega_0 + \delta\omega](t - t_0) + \Theta\} \tag{2}$$

where t_0 is the roundtrip time to the target. The time-delayed transmit replica $v_d(t)$ is given by

$$v_d(t) = a(t - t_d)\cos\{[\omega_0 + \delta\omega](t - t_d)\} \tag{3}$$

where t_d is the internal delay.

The cross-correlation of $v_r(t)$ and $v_d(t)$ yields a non-zero output only when $t_0 = t_d = t_{0d}$. Since the low-pass filter following the mixer discards the sum frequency signal at and around $2\omega_0$, the low-pass filtered mixer output $v_0(t)$ is given by

$$v_0(t) = \frac{1}{2}\Gamma a^2(t - t_{0d})\cos\Theta\,. \tag{4}$$

The average power in the received signal P_0 is then

$$P_0 = <v_0^2(t)>/R_0 = R_0 P_t^2 \Gamma^2 \cos^2\Theta\,. \tag{5}$$

Since the UWB reflectivity of the target is a function of frequency, i.e., $\Gamma = \Gamma(\omega)$ and $\Theta = \Theta(\omega)$, the average received power will yield a non-zero value. Also, since the magnitude and phase of the target reflectivity at the receiver output cannot be isolated, the system is not phase-coherent.

Phase coherence can be injected in noise radar by adding a frequency offset to the time-delayed transmit replica. This is called the heterodyne correlation noise radar, as shown in Figure 2. In this scheme, the reflected signal from the target is cross-correlated with a time-delayed and frequency-offset replica of the transmit waveform.

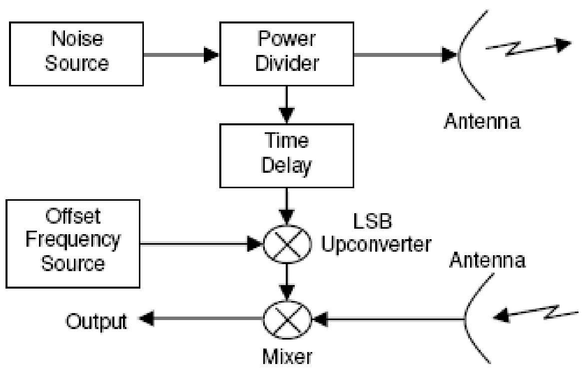

Figure 2: Block diagram of a heterodyne correlation noise radar.

In the heterodyne correlation case, the time-delayed and frequency-offset transmit replica $v_d(t)$ is now given by

$$v_d(t,\omega') = a(t-t_d)\cos\{[\omega_0 + \delta\omega - \omega'](t-t_d)\} \qquad (6)$$

where ω' is the frequency offset. The cross-correlation of $v_r(t)$ and $v_d(t,\omega')$ yields a non-zero output only when, as before, $t_0 = t_d = t_{0d}$. The low-pass filtered mixer output $v_0(t,\omega')$ is a signal centered exactly at ω' at all times, given by

$$v_0(t,\omega') = \frac{1}{2}\Gamma a^2(t-t_{0d})\cos[\omega' t + \Theta]\,. \qquad (7)$$

If this output is connected to an in-phase/quadrature (I/Q) detector (not shown) fed by the offset frequency generator, we can obtain the in-phase and quadrature outputs v_{0I} and v_{0Q}, respectively, given by

$$v_{0I} \propto \Gamma\cos\Theta\,, \qquad (8a)$$

$$v_{0Q} \propto \Gamma\sin\Theta\,. \qquad (8b)$$

The magnitude Γ and phase angle Θ of the target reflectivity can then be easily obtained from the above. Thus, the heterodyne correlation noise radar is indeed phase coherent and can be used in applications requiring coherence, such as polarimetry, interferometry, Doppler estimation, and SAR/ISAR imaging. Since the correlator output is always at the offset frequency ω', the UWB transmit waveform clearly collapses to a single frequency in the receiver. The detection bandwidth at correlator output can thus be reduced to enhance the signal-to-noise ratio (SNR). Doppler, if any, will modulate the correlator output and can be extracted from the I/Q detector.

4. WALL MATERIAL CONSIDERATIONS

Wall dielectric constant is a parameter that greatly affects through-wall sensing. Most wall materials in use are wood, concrete, glass, and stone. Although these are low loss dielectric materials, there may be situations where the transmission loss through walls may be high at specific frequency bands. A typical example is wave propagation through concrete walls containing reinforced bars (rebars). The rebar pattern causes transmission minima at specific frequencies whose periodicity is determined by the rebar spacing and wall thickness. At other frequencies approximately midway between the nulls, the propagation loss is very low. In order to overcome the transmission troughs caused by resonances at frequencies that are not known *a priori*, a wideband signal is an obvious choice. Transmitting such a signal ensures that at least some of the energy will get through the wall and permit the processing of target reflected signals.

The measure of radar's performance is captured in its receiver operating characteristics (ROC). We assume a known radar cross section (RCS) for the average human, based upon which a suitable threshold is set for the received signal. A false alarm occurs when a high noise spike triggers the threshold, while a missed detection is caused when a low signal value fails to trigger the threshold. False alarms and missed detections are also affected by external interference and other receiver noise (uncorrelated with the noise that is transmitted). We develop a Neyman-Pearson criterion in order to derive the probability of false alarm P_f and probability of detection P_d. Suitable hypotheses are created and a likelihood ratio test performed. Hypothesis H_0 representing the absence of a human or the presence of noise alone, is formed by subtracting the real-time background interferences from the average background interference. All background interferences are assumed to be uncorrelated and Gaussian. Hypothesis H_1 represents the presence of a human in background noise.

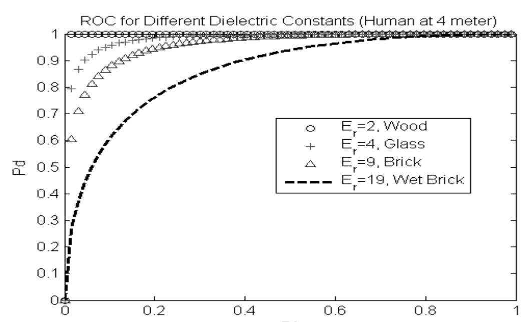

Figure 3: ROC curves for different wall dielectric constants for human at distance of 4 meters.

Using the above, we can generate suitable ROC curves. The wall dielectric constant affects through-wall detection performance. We considered the following wall materials: wood, concrete, glass, and stone. Simulated ROC curves are shown in Figure 3 for a human located 4 m behind the wall for a wall thickness of 30 cm. Strong reflections from the front air-wall and rear wall-air interfaces obscure the target reflections, also causing missed detections or false alarms.

The higher the dielectric constant, higher is the wall reflectivity, and lower is the energy transmitted through. We can generally achieve a false alarm probability of 0.2 (20%) for a detection probability of greater than 0.95 (95%).

5. HUMAN ACTIVITY CHARACTERIZATION

Various parts of the human body have different movements when a person is performing different physical activities. There is a need to remotely detect and recognize specific human activities for applications involving hostage liberation and search-and-rescue. The Doppler analysis of biometric radar signal is more complicated than a moving target having a constant speed and direction. A heartbeat radar signal has been described by a harmonic function containing fluctuations from skin and tissue. Although any human body movement can be modeled in this manner, this function is linear and stationary. However, mechanistic studies have shown that human body motion is usually nonlinear and nonstationary. While most time-frequency algorithms are only able to estimate linear and stationary signals, the Hilbert-Huang Transform (HHT) is able to analyze such nonlinear and nonstationary signals [5].

The HHT is a novel nonlinear and nonstationary signal analysis technique based on the combination of the empirical mode decomposition (EMD) and the Hilbert spectral analysis (HAS). The EMD identifies intrinsic oscillatory modes by their characteristic time scales in the data empirically. It separates the intrinsic mode functions (IMFs) from the original signal one by one, until the residue is monotonic. The original signal is thus decomposed into a finite and a small number of IMFs, where an IMF is any function with the same number of extrema and zero crossings, with symmetric envelopes. Using the EMD, we can identify and extract the specific IMFs which contain useful Doppler information and discard the IMFs which contain clutter and noise. The extracted IMFs all admit well-behaved Hilbert transforms. This time-frequency distribution of the amplitude is designated as the Hilbert amplitude spectrum, or simply the Hilbert spectrum. By plotting the Hilbert spectrum of the desired IMFs which are extracted using EMD, we can obtain the instantaneous Doppler frequencies. This new spectrum possesses much better time and frequency resolution.

Our experimental results using a 1-2 GHz noise radar with a 2-GHz single tone signal concealed within are shown in Figure 4 (no human) and Figure 5 (human present). The human was located behind a 30-cm concrete wall. For IMF8 in no-human data, shown in Figure 4, the power level and peak amplitudes are 3-dB lower than for the corresponding IMF8 in human breathing data, shown in Figure 5. For the no-human data, there are several peaks with comparable peak powers from 0.4-0.8 Hz, with no one truly dominant. The power level of human breathing IMF8 is the highest among other IMFs shown in Figure 5. We observe peaks that are close to this major 0.65-Hz peak at 0.5 Hz and 0.75 Hz. The peak count of IMF8 is between 10 and 15. This range of the peak values can be determined by the manual threshold in Figure 5. Our actual breathing count over the 20-second measurement period is 14, which is clearly within the range of the peak count. Additional averaging may improve the detection of human breathing.

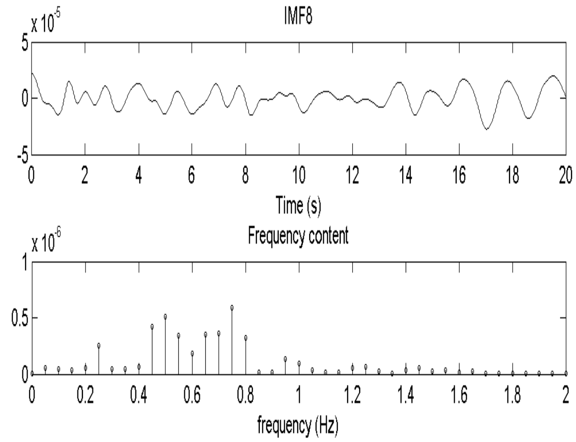

Figure 4: IMF8 and FFT of no-human data with noise-like signal.

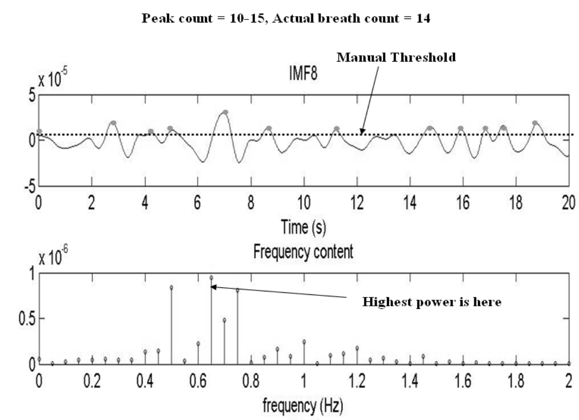

Figure 5: IMF8 and FFT of human breathing data using noise-like signal.

6. REFERENCES

[1] J.B. Tsui, *Digital Techniques for Wideband Receivers*, 2nd ed., Artech House, Boston, MA, 2001.

[2] L. Turner, "The evolution of featureless waveforms for LPI communications," *Proc. IEEE NAECON*, Dayton, OH, pp. 1325-1331, May 1991.

[3] B. M. Horton, "Noise-modulated distance measuring systems," *Proc. IRE*, vol. 47, no. 5, pp. 821-828, May 1959.

[4] M. P. Grant, G. R. Cooper, and A. K. Kamal, "A class of noise systems," *Proc. IEEE*, vol. 51, no. 7, pp. 1060-1061, July 1963.

[5] N.E. Huang, et al., "The empirical mode decomposition and the Hilbert spectrum for nonlinear and non-stationary time series analysis," *Proc. Royal Soc. London Ser. A - Mathematical Physical and Engineering Sciences*, vol. 454, pp. 903-995, Mar. 1998.